Nanoscale RSCPublishing

ARTICLE

Preparation and Characterization of Few-layer MoS_2 Nanosheets and Its Good Nonlinear Optical Response in PMMA Matrix

Cite this: DOI: 10.1039/x0xx00000x

Received 00th January 2014,
Accepted 00th January 2014

DOI: 10.1039/x0xx00000x

www.rsc.org/

Lili Tao[a#], Hui Long[a#], Bo Zhou[a#], Siu Fung Yu[a], Shu Ping Lau[a], Yang Chai[a], Kin Hung Fung[a], Yuen Hong Tsang[a]*, Jianquan Yao[b,c] and Degang Xu[b,c]*

Due to the relatively weak van der Waals (VDW) force between interlayers, few-layer MoS_2 nanosheets are prepared using simple ultrasonic exfoliation method and incorporated in PMMA. The good nonlinear optical (NLO) property of the MoS_2/PMMA composite for the nanosecond pulsed laser at both 532 and 1064 nm has been first reported. The size, thickness and atomic structure of MoS_2 nanosheets have been characterized by transmission electron microscopy (TEM) and atomic force microscopy (AFM). The interesting dependence of interlayer separation with respect to the layer number of MoS_2 has been successfully quantified. The average interlayer separation of the MoS_2 nanosheets increases and deviates much from the theoretical value of 0.31 nm with reducing the layer number. Such few-layer MoS_2 nanosheets have been homogeneously incorporated into solid-state PMMA, which shows low optical limiting thresholds, 0.4 and 1.3 J/cm^2, low limiting differential transmittance (T_C), 2% and 3% for the nanosecond laser operating at 532 nm and 1064 nm, respectively. The results suggest that MoS_2 nanosheets incorporated PMMA is a promising candidate of solid NLO material for optical limiting application.

Introduction

Recently, thin two-dimensional (2D) layer materials such as graphene,[1–3] hexagonal boron nitride (h-BN)[4,5] and layer transition metal dichalcogenides (LTMDs)[6-10] have attracted substantial attention due to their favourable electrical and optical properties. MoS_2 is one type of LTMDs materials with a sandwiched structure consisted of an atomic plane of molybdenum between two atomic planes of sulfur. The distance between the neighbouring S-Mo-S layers is 0.62 nm,[11] much larger than that of the carbon layers (0.34 nm) in graphite,[12] leading to weaker van der Waals (VDW) force between inter-layers. This makes thin layer MoS_2 sheet easier to be separated from bulk MoS_2. Various physical and chemical methods such as mechanical cleavage,[11,13-15] electrochemical Li-intercalation exfoliation,[16,17] and ultrasonic exfoliation[18,19] have been developed for this purpose. Among these methods, ultrasonic exfoliation has been employed in this research due to its relatively simple and scalable feature.

It has been demonstrated that the energy band structure of MoS_2 changes from indirect to direct bandgap owing to the electron motion confinement and the absence of interlayer perturbation in monolayer MoS_2 when it is thinned from bulk to monolayer, resulting in the emergence of the characteristic absorption peaks which can not be observed in the bulk MoS_2 and also a great improvement of photoluminescence.[15,17,20] Such interesting optical transition has attracted much attention, and the electrical and photoluminescence properties of thin MoS_2 have been studied extensively.[15,21-23] However, there has been not much research work done on its nonlinear optical (NLO) properties up to now, except for the ultrafast saturable absorption property of few-layer MoS_2 reported by K. P. Wang *et al,*[24] and reverse saturable absorption of graphene/MoS_2 composite at 532 nm reported by Q. Y. Ouyang *et al*.[25] Nowadays, high energy Q-switched nanosecond lasers operating at 1064 nm and frequency doubled into 532 nm are readily available and very popular for various commercial, industrial and military applications. Therefore, it becomes critically emergent and significant to explore novel and excellent NLO materials capable of protecting human eyes, detectors, sensors and cameras from high power laser damage for these laser systems. Few-layer MoS_2 shows strong absorption at 266 nm and 532 nm, indicating the high chance of two-photon absorption (TPA) at 532 nm (half the energy of 266 nm) and 1064 nm (half the energy of 532 nm). Thus, MoS_2 can be potentially better optical limiter for its high transmission at low intensity and high absorption for its TPA at high pumping intensity for most of commercially available high power laser operating around 1 μm and its frequency doubled wavelength around 0.5 μm, e.g., Yb fiber laser and Nd:YAG crystal lasers.[26-30]

Currently, NLO properties of 2D carbon materials such as graphene, graphene oxide (GO) and reduced graphene oxide (RGO) are being studied intensively.[31-33] GO is usually obtained from graphite by using Hummer's method. In detail, the graphite is pretreated with a lot of strong oxidant, such as $KMnO_4$, concentrated

H_2SO_4, H_2O_2 and so on, to decrease the connection between the carbon layers, and followed by ultrasonic treatment, to finally obtain the resultant thin GO sheets.[34,35] RGO is prepared by reducing the GO with reductants such as $NaBH_4$ and N_2H_4,[32] however, the fabrication processes are complicated, dangerous and unfriendly to the environment. Graphene sheets can be obtained from graphite just by ultrasonic exfoliation method.[36] Considering the much larger interlayer distance of MoS_2 than graphite, the thin MoS_2 sheets can be obtained more easily through the simple ultrasonic exfoliation method. Therefore, it is very meaningful to explore NLO properties of these thin MoS_2 sheets and its potential photonic applications. Optical limiters can be in liquid or solid form, but the liquid based has very limited practical use due to its high rate of evaporation and contamination, leakage caused by container damage, high losses originating from the refractive index mismatch between the liquid and solid interfaces, relatively easy aggregation as well as the lack of flexibility and stability. Thin film based optical limiters have very short absorption length and easy to be damaged. Therefore, it is better to incorporate the NLO materials into bulk solid state optical matrix so as to stabilize and isolate it from outside environment, which offers more advantages e.g., withstanding higher optical power, avoiding aggregation and well suitable for producing commercial photonics products.

In this work, we incorporate few-layer MoS_2 in solid PMMA matrix to isolate it from outside environment and avoid the oxidization. The fabricated MoS_2/PMMA composite shows good NLO properties. To our best knowledge, there has been no report on this so far. The few-layer MoS_2 nanosheets are obtained through ultrasonic exfoliation of the powder synthesized by hydrothermal method in advance. Transmission electron microscopy (TEM) and atomic force microscopy (AFM) results indicate that the prepared MoS_2 sheets are very thin (<5 layers), and an interesting phenomenon is found that the interlayer separation depends a lot on the layer number. The few-layer MoS_2 nanosheets are well homogeneously incorporated in PMMA matrix without any complicated functionalization like graphene.[37] PMMA is a good optical host material with advantages such as high optical transparency, excellent mechanical property, low cost, moldable and so on, and more significantly, it shows good and stable NLO property, demonstrating its great potential acting as a novel NLO material for optical limiting application.

Experimental

Hydrothermal preparation of small MoS_2 powder

Hydrothermal preparation of MoS_2 has been previously reported using $(NH_4)_2MoS_4$ as raw material.[38] In our experiment, $Na_2MoO_4 \cdot H_2O$ (0.3 g) and $CS(NH_2)_2$ (0.4 g) were dissolved in DI water (30 mL) under vigorous stirring, followed by transferring the transparent solution to a 50-mL-capacity Teflon autoclave and keeping it at 240 °C for 24 hours. After hydrothermal process, the formed black suspension was centrifuged and washed with DI water several times and dried at 60 °C in vacuum. Finally, black MoS_2 crystalline powder was obtained.

Preparation of MoS_2/PMMA bulk

Few-layer MoS_2 nanosheets were first obtained by ultrasonic exfoliation method. MoS_2 (16 mg) powder was dispersed in N-methyl-2pyrrolidone (NMP, C_5H_9NO, 80 mL) under vigorous stirring, followed by ultrasonic treatment for 18 h, and then the suspension was centrifuged at 3000 rpm for 20 min to remove the thick MoS_2 nanosheets. The left MoS_2 suspension was kept for incorporation into PMMA. MMA (20 mL) and MoS_2 suspension were first mixed and heated at 75 °C for 10 min, and then BPO (0.023 g) was added and heated at 75 °C for another 10 min. Followed by heat treatment at 105 °C for 20 min. Finally, it was kept at 75 °C for 30 h and solid transparent MoS_2/PMMA was obtained. The incorporated MoS_2 concentrations in MoS_2/PMMA-1 and MoS_2/PMMA-2 are about 0.008 mg/cm^3 and 0.016 mg/cm^3, respectively.

Characterization

X-ray diffraction (XRD) pattern was recorded using a Rigaku SmartLab X-ray diffractometer. The microstructure and chemical composition were investigated using a field emission transmission electron microscopy (FETEM, JEOL Model JEM-2100F), equipped with an energy dispersive spectrometer (EDS). The surface morphology and height information of samples were obtained by the atomic force microscopy (AFM, Veeco Nanoscope V). The Raman spectrum measurement was carried out on a HR-800 Raman spectrometer with argon ion laser emitted at 488 nm. Photoluminescence spectra were obtained using an Edinburgh Instruments FLS920 Steady-State and Time Resolved Fluorescence Spectrometer equipped with a photomultiplier tube (PMT) for visible fluorescence. UV-Vis absorption spectra were recorded on a SHIMADZU UV-2550 UV-Vis spectrophotometer. The NLO properties were examined by open aperture z-scan method using a 8 ns pulsed Nd:YAG laser operating at a repetition of 10 Hz.

Results and Discussion

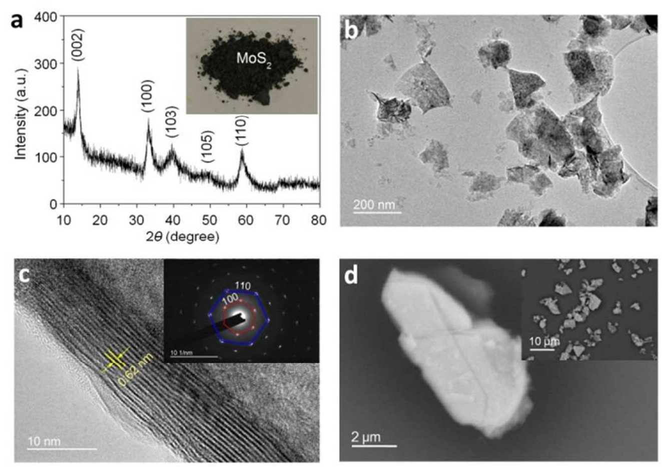

Figure 1. (a) XRD pattern, (b) TEM and (c) HRTEM images of as-prepared MoS_2. Inset of (a) is the digital photo of MoS_2 powder. Inset of (c) is the SAED pattern of the MoS_2 sheet. (d) SEM image of the commercial MoS_2 bought from Aladdin-Reagent Company. Inset is the SEM image with lower magnification.

Figure 1a shows the X-ray diffraction pattern of the MoS_2 prepared by hydrothermal method, which is black powder as shown in the inset. The diffraction peaks located at 2θ = 14°, 33°, 40°, 50°, 59° correspond to the planes of (002), (100), (103), (105) and (110), respectively, agreeing well with the hexagonal MoS_2 (JCPDS card No. 37-1492). Figure 1b displays the TEM image of the MoS_2 obtained through hydrothermal method, with the flake size of around 200 nm. From the HRTEM image (Figure 1c), it can be found that the obtained MoS_2 nanosheet is ~16 layers thick, and the interlayer separation is determined to be 0.62 nm, identical to the theoretical layer distance along the c-axis direction.[11] The selected area electron diffraction (SAED) pattern of the MoS_2 nanosheet is presented in Figure 1c inset that reveals the hexagonal lattice structure and well stacked single crystal layer feature, with the mark of the diffraction points ascribed to the (100) and (110) planes. Figure 1d shows the SEM image of MoS_2 powder bought from Aladdin-Reagent Company, showing its flake size of several micrometers, much larger than the MoS_2 sheets obtained through hydrothermal method. The large size starting material is unfavourable to obtaining thin MoS_2 nanosheets through ultrasonic exfoliation, which has been confirmed by the K. P. Wang *et al*.[24] In their work, MoS_2 sheets with large size (hundreds of nanometers) and thickness (dozens of nanometers) were obtained from large commercial MoS_2 powder as starting material. It is well known that the thinner MoS_2 is, the stronger optical response will be obtained.[21,39] And, moreover, the MoS_2 sheets need to be small enough for a perfect dispersion in liquid and solid matrix aiming to minimize the optical scattering losses. Therefore, using small raw MoS_2 powder prepared through hydrothermal method has the edge over using large commercially available MoS_2.

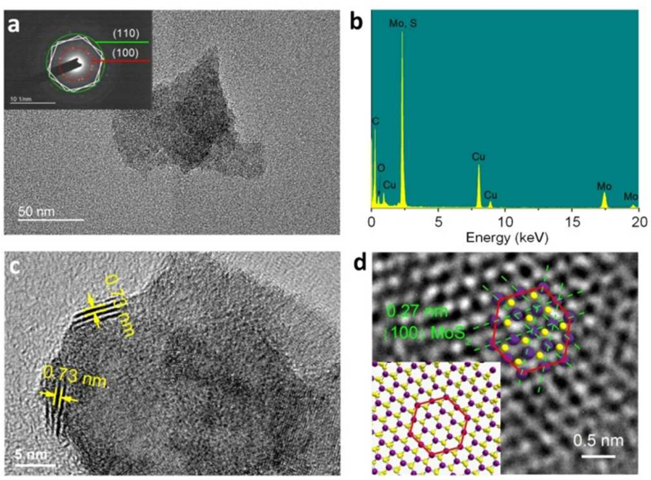

Figure 2. (a) Low-magnification TEM image of MoS_2 nanosheets obtained after ultrasonic exfoliation, inset shows the SAED pattern. (b) EDS spectrum of MoS_2 nanosheets. (c) HRTEM image showing layer information of the MoS_2 sheets. (d) HRTEM image indicating atomic structure of MoS_2, inset illustrates the schematic structure with yellow and purple balls corresponding to S and Mo atoms, respectively.

As is well known, the connection between the S-Mo-S layers is weak VDW force, making it easy to be separated. In this study, few-layer MoS_2 is obtained by employing ultrasonic exfoliation method. Figure 2a shows the TEM image of the MoS_2 nanosheets after 18 h ultrasonic treatment, demonstrating obtained MoS_2 below 100 nm. As analyzed from the SAED pattern given in Figure 2a inset, the multi-group hexagonal diffraction points with a certain angle misplace indicate that the MoS_2 sheets consist of several few-layer single crystal MoS_2 stacked in different orientations. The elemental composition of the sheets is confirmed by energy dispersive spectrometer (EDS) result shown in Figure 2b, and the Cu peak recorded is due to the copper mesh support for measurement.

It has been recognized as a common method to determine the layer number of 2D layer material from the HRTEM image of the folded edge.[40,41] As directly evidenced from the folded edge in Figure 2c, the obtained MoS_2 nanosheets through 18 h ultrasonic exfoliation contains three layers. Figure 2d shows the HRTEM image of MoS_2 at the atomic scale, the large black points are Mo atoms and the small black points are S atoms; they are marked by purple balls for Mo atoms and yellow balls for S atoms, respectively. The 0.27 nm interplane distance matches well with the (110) planes, indicating a top view through c-axis direction. As shown in Figure 2d inset, the corresponding atomic structural model viewing through c-axis direction can foster deep understanding of the MoS_2 structure indicated by the high resolution TEM image.

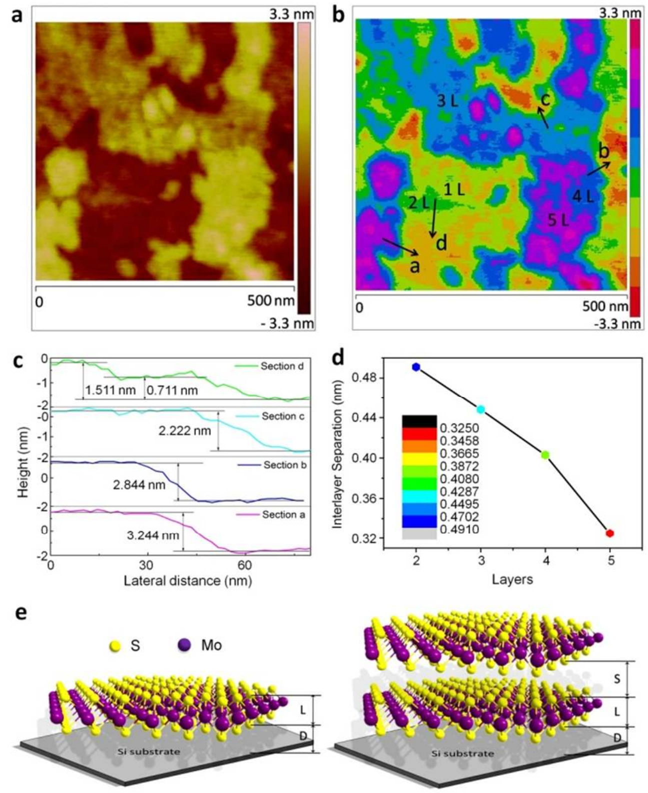

Figure 3. (a) 2D topographical and (b) 2D stepped height-type AFM images of few-layer MoS_2 nanosheets. (c) Height profiles of the sections marked in (b). (d) Interlayer separation dependence on the layer number. (e) Schematic diagram of monolayer and double layer MoS_2 on Si substrate. (L: the thickness of S-Mo-S layer; D: the distance from MoS_2 to the substrate; S: the separation between the S-Mo-S layers.)

Figure 3a shows the 2D AFM topographical image of the MoS_2 nanosheets with thickness below several nanometers obtained after 18h ultrasonic exfoliation, confirming again the successful preparation of thin MoS_2 nanosheets through ultrasonic treatment. With clearly observable difference of thickness, the layer number is definitely labelled in the stepped height-type AFM image (Figure 3b). In order to precisely analyze the thickness of the areas with different colours, the height profiles of the sections marked in Figure 3b are plotted in Figure 3c, with the precise thickness given in it. In fact, the measured thickness of MoS_2 is a summation of three contributions: the distance from MoS_2 to the substrate (D), the height of S-Mo-S layers (L) and the interlayer separations (S). Taking the bi-layer MoS_2 for an example, the measured thickness equals to D+2L+S, where L is 3.08 Å,[11] and D is determined to be 4.03 Å according to the measured thickness of monolayer MoS_2. And then, the interlayer separations of MoS_2 with different layers are obtained and plotted in Figure 3d. It is interesting to find that the interlayer separation is much closer to the theoretical value 0.31 nm[11] as the layer number increase, and much larger when it contains fewer layers. This is similar as the few-layer graphene reported by Y. X. Ni *et al*.[42] As the connection between the S-Mo-S layers comes from VDW force, the larger interlayer separation of thinner MoS_2 can be ascribed to the weaker attractive VDW force between the layers because of the fewer atoms, as well as the increased interlayer repulsive force due to the active edge effect of the smaller nanosheets.[43,44] Figure 3e shows the schematic structure of mono- and bi-layer MoS_2 sheet. For the monolayer MoS_2, the measured thickness is exactly the summation of the S-Mo-S bond distance (L) and the distance between MoS_2 and the substrate (D), as L is 3.08 Å and the D is variable. This explains why the thickness of single layer MoS_2 deviates largely in different works (i.e., changing from 0.5 to 0.9 nm).[11,39,45,46]

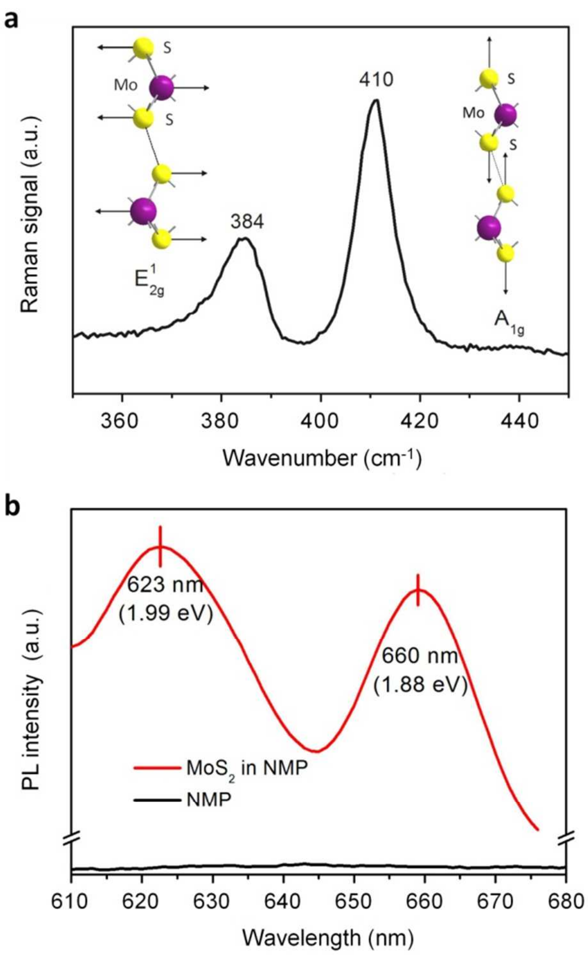

Figure 4. (a) Raman spectrum and (b) Photoluminescence spectrum of MoS_2 nanosheets obtained after ultrasonic exfoliation. Insets of (a) show the schematic of the vibration modes at 384 cm^{-1} (left) and 410 cm^{-1} (right).

The Raman spectrum of the MoS_2 sheets obtained after 18 h ultrasonic exfoliation is given in Figure 4a. The two characteristic vibration modes $\mathbf{E}_{2g}^1$ (in-plane) and A_{1g} (out-of-plane) located at 384 and 410 cm^{-1}, respectively, are observed. The locations of these two peaks are in agreement with the few-layer MoS_2 reported.[21] The full-width-half-maximum (FWHM) of $\mathbf{E}_{2g}^1$ and A_{1g} bands are calculated to be 10.2 and 7.4 cm^{-1}, respectively, much broader than other reported results.[39,46,47] It has been recognized widely that the locations of $\mathbf{E}_{2g}^1$ and A_{1g} peaks of MoS_2 show a little shift with varying layers: $\mathbf{E}_{2g}^1$ shifts to higher frequency while A_{1g} shifts to lower frequency for thinner MoS_2.[22,47,48] Therefore, the broader FWHM of Raman spectrum also indicates the co-existence of MoS_2 nanosheets with different layers. Figure 4b shows the photoluminescence spectrum of MoS_2 in NMP under 532 nm excitation. The two characteristic emission peaks located at 623 and 660 nm are ascribed to the B and A direct excitonic transitions from the lowest conduction band to the highest spin-split valence band at the K-point of the Brillouin zone,[15,39] respectively, indicating that the layer number of MoS_2 has been successfully reduced and it has become a direct gap semiconductor.

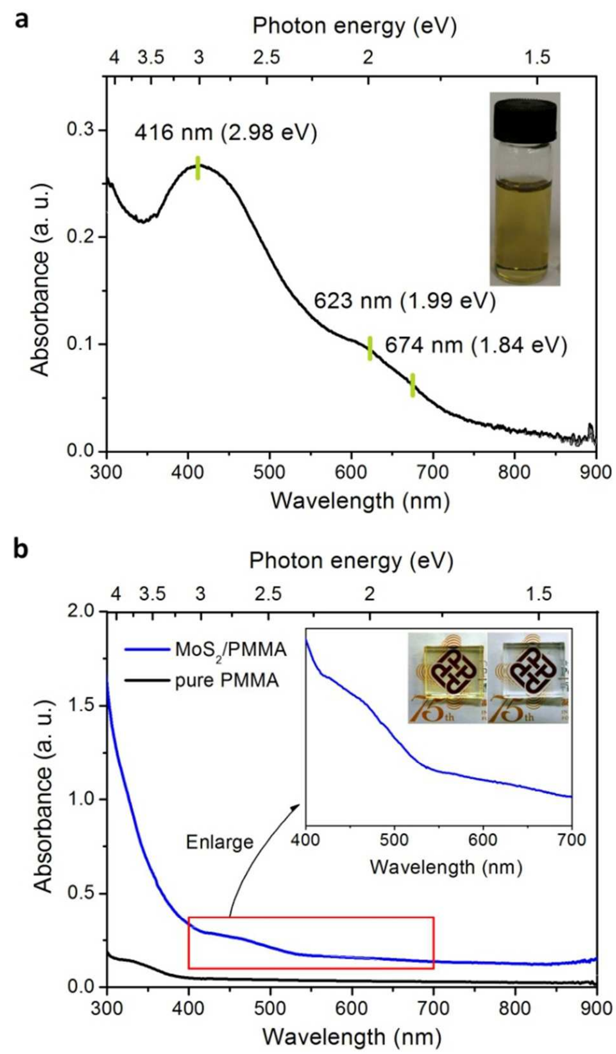

Figure 5. (a) Absorption spectrum of the few layer MoS_2 suspension in NMP. Inset shows the digital photo of such sample. (b) Absorption spectra of pure PMMA and MoS_2/PMMA composite bulks. Insets show the enlarged absorption within 400-700 nm region, and digital photos of MoS_2/PMMA (left) and PMMA (right).

The absorption spectrum of the few-layer MoS_2 nanosheets suspension in NMP is shown in Figure 5a. It can be observed that the two characteristic absorption peaks at 623 nm (1.99 eV) and 674 nm (1.84 eV) arise from direct transition from valance band to conduction band at the K-point of the Brillouin zone, known as the B and A transitions, respectively,[8,15,17,24] are recorded. Such two peaks with little energy difference is due to the spin-orbital splitting of the valence band.[15,24] In addition, the broad absorption band centered at 416 nm (2.98 eV) arising from the complicated C and D transitions is also observed.[17,18,24] As shown in Figure 5a inset, the suspension shows the characteristic yellow-green color of few-layer MoS_2, similar to other reports.[17,18] The above results have confirmed that few-layer MoS_2 nanosheets are obtained through ultrasonic exfoliation in this contribution, agreeing well with the above TEM and AFM analysis. The MoS_2 nanosheets have been incorporated in PMMA, the well known organic optical glass, in order to realize various optical applications such as saturable absorber, optical limiter and so on. Figure 5b gives the absorption spectra of pure PMMA and MoS_2/PMMA composite bulks, the characteristic absorption peaks between 400-700 nm corresponding to MoS_2 are recorded. And the homogeneous yellow-green colour (see Figure 5b inset) indicates that MoS_2 has been not only successfully incorporated into PMMA matrix but also in a homogeneous dispersion.

Figure 6a and 6b show the plots of output fluence F_{out} versus input fluence F_{in} for PMMA and MoS_2/PMMA composite bulks measured at 532 and 1064 nm, respectively. The ratio F_{out}/F_{in} in the limit of zero fluence gives the linear transmittance (T_L), and the values are shown in Table 1. The measured results reveal that the transmittance of MoS_2/PMMA remains the same initially and then decreases with the increase of the input fluence at both 532 and 1064 nm, showing the typical feature of optical limiting materials. In contrast, only linear optical property observed in pure PMMA reveals that PMMA has no contribution to the NLO response of MoS_2/PMMA composite. The NLO onset threshold (F_{ON}) and optical limiting threshold (F_{OL}, defined as the input fluence point at which the normalized transmittance drops to 50%) are vital parameters to evaluate the NLO performance of a given material. Herein F_{ON} and F_{OL} values are determined and listed in Table 1. For the sample MoS_2/PMMA-2, F_S are 0.01 J/cm^2 and 0.04 J/cm^2, and F_{OL} are 0.40 J/cm^2 and 1.30 J/cm^2 for MoS_2/PMMA at 532 nm and 1064 nm, respectively. Although these thresholds are higher than the single-layer graphene dispersion,[2] they are much lower than or comparable to other NLO materials including few-layer graphene,[32,49,50] grapheme oxide,[32,34,51,52] reduced graphene oxide,[52] carbon nanotube[32,53-55] and various metal nanostructures,[56-58]. At high input fluence, the slope dF_{out}/dF_{in} gives the limiting differential transmittance (T_C), indicating the output clamping characteristics of samples. T_C for the sample MoS_2/PMMA-2 are 2% and 3% at 532 nm and 1064 nm, respectively, even lower than the single-layer graphene dispersion, further indicating its better optical limiting performance.[2] All these results suggest that MoS_2/PMMA composite has great potential as a type of excellent NLO material for optical limiting applications.

Two-photon absorption (TPA) and nonlinear scattering (NLS) have been acknowledged as the dominant mechanisms for NLO properties of optical limiting materials. Since NLS is usually resulted from the bubbles formed in the solution based NLO materials, it is reasonable to assume that TPA process makes dominant contribution to the NLO performance of solid-state MoS_2/PMMA composite bulk. And the TPA coefficient (β) subsequently can be obtained by the following equation:[59]

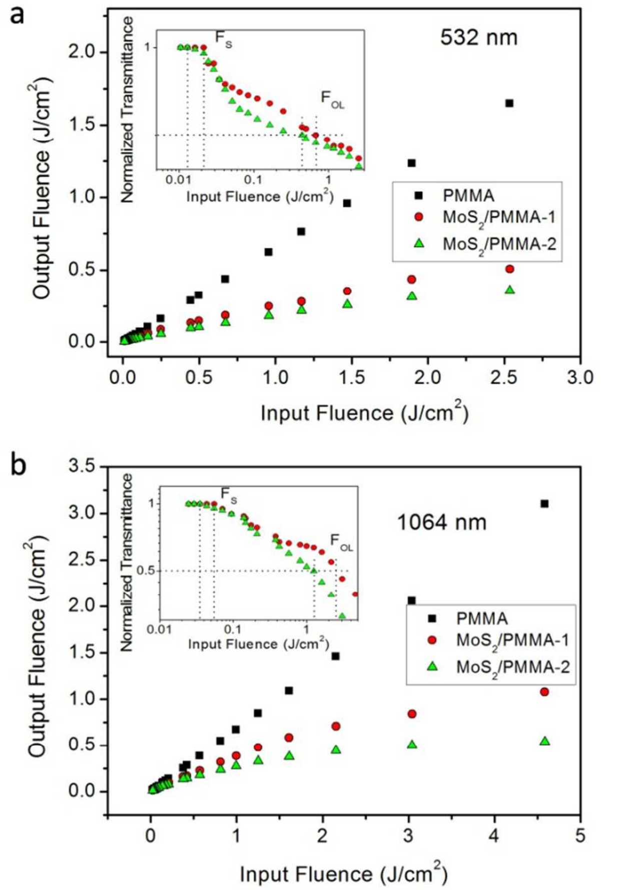

Figure 6. The output fluence dependence on the input fluence at 532 nm (a) and 1064 nm (b), respectively. Insets are the corresponding normalized transmittance dependence on the input fluence. The concentration of MoS_2 in MoS_2/PMMA-1 and MoS_2/PMMA-2 are 0.008 and 0.016 mg/cm^3, respectively.

$$I_0 = \frac{I_i e^{-\alpha L}}{1+\left(1-e^{-\alpha L}\right)\beta I_i \big/ 2\sqrt{2}\alpha}, \qquad (1)$$

where I_i and I_o are the input and output laser power respectively, α is the linear absorption coefficient, and L is the path length. The β values are fitted and given in Table 1. Such β values are larger than or compatible to the carbon materials,[34,60-62] indicating efficient TPA process in such MoS_2/PMMA composite bulk at both 532 and 1064 nm and hence leading to good NLO performance for optical limiting application.

Table 1. Optical parameters of Linear transmittance (T_L), limiting differential transmittance (T_C), two-photon absorption coefficient (β), NOL onset thresholds (F_{ON}) and optical limiting thresholds (F_{OL}) for MoS_2/PMMA composites.

Samples	532 nm					1064 nm				
	T_L (%)	T_C (%)	β (cm·GW^{-1})	F_{ON} (J·cm^{-2})	F_{OL} (J·cm^{-2})	T_L (%)	T_C (%)	β (cm·GW^{-1})	F_{ON} (J·cm^{-2})	F_{OL} (J·cm^{-2})
MoS_2/PMMA-1	55	11	62	0.02	0.7	60	15	27	0.06	2.3
MoS_2/PMMA-2	44	2	70	0.01	0.4	53	3	55	0.04	1.3

Note: The concentration of MoS_2 in MoS_2/PMMA-1 and MoS_2/PMMA-2 are 0.008 and 0.016 mg/cm^3, respectively.

Conclusions

In conclusion, good NLO property of the novel 2D material MoS_2 at both 532 and 1064 nm is studied and reported in this contribution. By employing ultrasonic exfoliation method, few-layer MoS_2 sheets are successively prepared. The interlayer separation in such few-layer MoS_2 has an interesting dependence on the layer number, primarily due to the weaker van de Waals force and increased interlayer repulsive force resulted from the active edge effect of the smaller nanosheets. Z-scan results of MoS_2/PMMA composite bulk further demonstrate the low NLO onset threshold F_{ON}, low optical limiting threshold F_{OL}, low optical limiting differential transmittance T_C, and high two-phonon absorption coefficient β at both 532 and 1064 nm, confirming the good NLO property. Hence, the few-layer MoS_2 nanosheets incorporated PMMA bulk can be a kind of novel NLO material with great potential for optical limiting applications.

Acknowledgements

This work is financially supported by the Research Grants Council of Hong Kong, China (Project Number: GRF PolyU 526511), the Hong Kong Innovation and Technology Fund: (Project Number: ITS/035/12), and the Hong Kong Polytechnic University (Project Number: G-YM44).

Notes and references

[a] Department of Applied Physics and Materials Research Center, The Hong Kong Polytechnic University, Hung Hom, Kowloon, Hong Kong. Email address: yuen.tsang@polyu.edu.hk

[b] The Institute of Laser & Optoelectronics, The College of Precision Instruments and Opto-Electronic Engineering, Tianjin University, Tianjin, 300072, China.

[c] Key Laboratory of Opto-Electronics Information and Technical Science (Ministry of Education), Tianjin University, Tianjin 300072, China. Email address: xudegang@tju.edu.cn

[#] These authors contributed equally to this work.

1. R. Lv, Q. Li, A. R. Botello-Mendez, T. Hayashi, B. Wang, A. Berkdemir, Q. Hao, A. L. Elias, R. Cruz-Silva, H. R. Gutierrez, *et al. Sci. Rep.*, 2012, **2**, 586.
2. G. Lim, Z. Chen, J. Clark, R. G. S. Goh, W. Ng, H. Tan, R. H. Friend, P. K. H. Ho, L. Chua, *Nat. Photonics*, 2011, **5**, 554.
3. Q. Bao, H. Zhang, Y. Wang, Z. Ni, Y. Yan, Z. X. Shen, K. P. Loh, D. Y. Tang, *Adv. Funct. Mater.*, 2009, **19**, 3077.
4. Z. Liu, L. Ma, G. Shi, W. Zhou, Y. Gong, S. Lei, X. Yang, J. Zhang, J. Yu, K. P. Hackenberg, *et al. Nat. Nanotechnol.*, 2013, **8**, 119.
5. I. Jo, M. T. Pettes, J. Kim, K. Watanabe, T. Taniguchi, Z. Yao, L. Shi, *Nano Lett.*, 2013, **13**, 550.
6. Y. Shi, J.-K. Huang, L. Jin, Y.-T. Hsu, S. F. Yu, L.-J. Li, H. Y. Yang, *Sci. Rep.*, 2013, **3**, 1839.
7. M. Chhowalla, H. S. Shin, G. Eda, L.-J. Li, K. P. Loh, H. Zhang, *Nat. Chem.*, 2013, **5**, 263.
8. K. F. Mak, K. He, C. Lee, G. H. Lee, J. Hone, T. F. Heinz, J. Shan, *Nat. Mater.*, 2013, **12**, 207.
9. X. Huang, Z. Zeng, H. Zhang, *Chem. Soc. Rev.*, 2013, **42**, 1934.
10. H. Li, J. Wu, X. Huang, G. Lu, J. Yang, X. Lu, Q. Xiong, H. Zhang, *ACS Nano*, 2013, **7**, 10344.
11. D. J. Late, B. Liu, H. S. S. R. Matte, C. N. R. Rao, V. P. Dravid, *Adv. Funct. Mater.*, 2012, **22**, 1894.
12. G. Eda, G. Fanchini, M. Chhowalla, *Nat. Nanotechnol.*, 2008, **3**, 270.
13. J. Wu, H. Li, Z. Yin, H. Li, J. Liu, X. Cao, Q. Zhang, H. Zhang, *Small*, 2013, **9**, 3314.
14. H. Li, X. Qi, J. Wu, Z. Zeng, J. Wei, H. Zhang, *ACS Nano*, 2013, *7*, 2842–2849.
15. A. Splendiani, L. Sun, Y. Zhang, T. Li, J. Kim, C.-Y. Chim, G. Galli, F. Wang, *Nano Lett.*, 2010, **10**, 1271.
16. C. Zhu, Z. Zeng, H. Li, F. Li, C. Fan, H. Zhang, *J. Am. Chem. Soc.*, 2013, **135**, 5998.
17. G. Eda, H. Yamaguchi, D. Voiry, T. Fujita, M. Chen, M. Chhowalla, *Nano Lett.*, 2011, **11**, 5111.
18. A. O'Neill, U. Khan, J. N. Coleman, *Chem. Mater.*, 2012, **24**, 2414.
19. J. N. Coleman, M. Lotya, A. O'Neill, S. D. Bergin, P. J. King, U. Khan, K. Young, A. Gaucher, S. De, R. J. Smith, *et al. Science*, 2011, **331**, 568.
20. K. F. Mak, C. Lee, J. Hone, J. Shan, T. F. Heinz, *Phys. Rev. Lett.*, 2010, **105**, 136805.
21. S. Tongay, J. Zhou, C. Ataca, K. Lo, T. S. Matthews, J. Li, J. C. Grossman, J. Wu, *Nano Lett.*, 2012, **12**, 5576.
22. K.-K. Liu, W. Zhang, Y.-H. Lee, Y.-C. Lin, M.-T. Chang, C.-Y. Su, C.-S. Chang, H. Li, Y. Shi, H. Zhang, *et al. Nano Lett.*, 2012, **12**, 1538.
23. Y. Y. Hui, X. Liu, W. Jie, N. Y. Chan, J. Hao, Y.-T. Hsu, L.-J. Li, W. Guo, S. P. Lau, *ACS Nano*, 2013, **7**, 7126.
24. K. Wang, J. Wang, J. Fan, M. Lotya, A. O'Neill, D. Fox, Y. Feng, X. Zhang, B. Jiang, Q. Zhao, *et al. ACS Nano*, 2013, **7**, 9260.
25. Q. Ouyang, H. Yu, H. Wu, Z. Lei, L. Qi, Y. Chen, *Opt. Mater.*, 2013, **35**, 2352.
26. D. Xu, Y. Wang, H. Li, J. Yao and Y. H. Tsang, *Opt. Express*, 2007, **15**,, 3991.
27. Y. H. Tsang, T. A. King, D. K. Ko, J. Lee, *Opt. Comm.*, 2006, **259**, 236.
28. Y. H. Tsang, T. A. King, T. Thomas, C. Udell, M. C. Pierce, *Opt. Comm.*, 2003, **215**, 381.
29. Y.-G. Wang, Z.-S. Qu, J. Liu, Y. H. Tsang, *IEEE J. Lightwave Technol.*, 2012, **30**, 3259.
30. L. Zhang, Y. G. Wang, H. J. Yu, W. Sun, Y. Y. Yang, Z. H. Han, Y. Qu, W. Hou, J. M. Li, X. C. Lin, Y. Tsang, *IEEE J. Lightwave Technol.*, 2012, **30**, 2713.,
31. J. Balapanuru, J.-X. Yang, S. Xiao, Q. Bao, M. Jahan, L. Polavarapu, J. Wei, Q.-H. Xu, K. P. Loh, *Angew. Chem. Int. Ed.*, 2010, **122**, 6699.
32. A. Midya, V. Mamidala, J.-X. Yang, P. K. L. Ang, Z.-K. Chen, W. Ji, K. P. Loh, *Small*, 2010, **6**, 2292.
33. Q. Bao, H. Zhang, J. Yang, S. Wang, D. Y. Tang, R. Jose, S. Ramakrishna, C. T. Lim, K. P. Loh, *Adv. Funct. Mater.*, 2010, **20**, 782.
34. J. Zhu, Y. Li, Y. Chen, J. Wang, B. Zhang, J. Zhang, W. J. Blau, *Carbon*, 2011, **49**, 1900.
35. X. Xu, D. Ou, X. Luo, J. Chen, J. Lu, H. Zhan, Y. Dong, J. Qin, Z. Li, *J. Mater. Chem.*, 2012, **22**, 22624.
36. T. Ramanathan, A. A. Abdala, S. Stankovich, D. A. Dikin, M. Herrera-Alonso, R. D. Piner, D. H. Adamson, H. C. Schniepp, X. Chen, R. S. Ruoff, *et al. Nat. Nanotechnol.*, 2008, **3**, 327.
37. Y. Hernandez, V. Nicolosi, M. Lotya, F. M. blighe, Z. Sun, S. De, I. T. Mcgovern, B. Holland, M. Byrne, Y. k. Gun'ko, J. J. Boland, P. Niraj, G. Duesberg, S. Krishnamurthy, R. Goodhue, J. Hutchison, V. Scardaci, A. C. Ferrari, J. N. Coleman, *Nat. Nanotechnol.*, 2008, **3**, 563.

38. Y. G. Li, H. L. Wang, L. M. Xie, Y. Y. Liang, G. S. Hong, H. J. Dai, *J. Am. Chem. Soc.*, 2011, **133**, 7296.
39. Y. H. Lee, X. Q. Zhang, W. Zhang, M. T. Chang, C. T. Lin, K. D. Chang, Y. C. Yu, J. T. W. Wang, C. S. Chang, L. J. Li, *et al. Adv. Mater.*, 2012, **24**, 2320.
40. L. Ci, L. Song, C. Jin, D. Jariwala, D. Wu, Y. Li, A. Srivastava, Z. F. Wang, K. Storr, L. Balicas, *et al. Nat. Mater.*, 2010, **9**, 430.
41. A. Reina, X. Jia, J. Ho, D. Nezich, H. Son, V. Bulovic, M. S. Dresselhaus, J. Kong, *Nano Lett.*, 2009, **9**, 30.
42. Y. Ni, Y. Chalopin, S. Volz, *Appl. Phys. Lett.*, 2013, **103**, 061906.
43. M. R. Karim, K. Hatakeyama, T. Matsui, H. Takehira, T. Taniguchi, M. Koinuma, Y. Matsumoto, T. Akutagawa, T. Nakamura, S. Noro, t. Yamada, H. Kitagawa, S. Hayami, *J. Am. Chem. Soc.*, 2013, **135**, 8097.
44. J. F. Xie, H. Zhang, S. Li, R. X. Wang, X. Sun, M. Zhou, J. F. Zhou, X. W. Lou, Y. Xie, *Adv. Mater.*, 2013, **25**, 5807.
45. J. Brivio, D. T. L. Alexander, A. Kis, *Nano Lett.*, 2011, **11**, 5148.
46. Y. Yu, C. Li, Y. Liu, L. Su, Y. Zhang, L. Cao, *Sci. Rep.*, 2013, **3**, 1866.
47. S. Najmaei, Z. Liu, P. M. Ajayan, J. Lou, *Appl. Phys. Lett.*, 2012, **100**, 013106.
48. Y. Zhan, Z. Liu, S. Najmaei, P. M. Ajayan, J. Lou, *Small*, 2012, **8**, 966.
49. M. Feng, R. Sun, H. Zhan, Y. Chen, *Nanotechnology*, 2010, **21**, 75601.
50. M. Feng, H. Zhan, Y. Chen, *Appl. Phys. Lett.*, 2010, **96**, 033107.
51. L. Tao, B. Zhou, G. Bai, Y. Wang, S. F. Yu, S. P. Lau, Y. H. Tsang, J. Yao, D. Xu, *J. Phys. Chem. C*, 2013, **117**, 23108.
52. T. He, X. Qi, R. Chen, J. Wei, H. Zhang, H. Sun, *Chempluschem*, 2012, **77**, 688.
53. M. Feng, R. Sun, H. Zhan, Y. Chen, *Carbon*, 2010, **48**, 1177.
54. X. Sun, R. Q. Yu, G. Q. Xu, T. S. Hor, W. Ji, *Appl. Phys. Lett.*, 1998, **73**, 3632.
55. P. Chen, X. Wu, X. Sun, J. Lin, W. Ji, K. Tan, *Phys. Rev. Lett.*, 1999, **82**, 2548.
56. R. West, Y. Wang, T. Goodson III, *J. Phys. Chem. B*, 2003, **107**, 3419.
57. H. Pan, W. Z. Chen, Y. P. Feng, W. Ji, J. L. Lin, *Appl. Phys. Lett.*, 2006, **88**, 223106.
58. L. Polavarapu, N. Venkatram, W. Ji, Q.-H. Xu, *ACS Appl. Mater. Interfaces*, 2009, **1**, 2298.
59. T. Boggess, K. Bohnert, K. Mansour, S. Moss, I. Boyd, A. Smirl, *IEEE J. Quantum Electron.*, 1986, **22**,360.
60. S. Husaini, J. E. Slagle, J. M. Murray, S. Guha, L. P. Gonzalez, R. G. Bedford, *Appl. Phys. Lett.*, 2013, **102**, 191112.
61. Z. Liu, Y. Wang, X. Zhang, Y. Xu, Y. Chen, J. Tian, *Appl. Phys. Lett.*, 2009, **94**, 021902.
62. X.-L. Zhang, X. Zhao, Z.-B. Liu, S. Shi, W.-Y. Zhou, J.-G. Tian, Y.-F. Xu, Y.-S. Chen, *J. Opt.*, 2011, **13**, 075202.